Quantum many-body thermal machines enabled by atom-atom correlations

R. S. Watson and K. V. Kheruntsyan
School of Mathematics and Physics, University of Queensland, Brisbane, Queensland 4072, Australia
(Dated: March 4, 2024)

Particle-particle correlations, characterized by the second-order Glauber correlation function, play an important role in the understanding of various phenomena in radio and optical astronomy, quantum and atom optics, particle physics, condensed matter physics, and quantum many-body theory. However, the relevance of such correlations to quantum thermodynamics has so far remained illusive. Here, we propose and investigate a class of quantum many-body thermal machines whose operation is directly enabled by second-order atom-atom correlations in an ultracold atomic gas. More specifically, we study quantum thermal machines that operate in a sudden interaction-quench Otto cycle and utilize a one-dimensional Lieb-Liniger gas of repulsively interacting bosons as the working fluid. The atom-atom correlations in such a gas are different to those of a classical ideal gas, and are a result of the interplay between interparticle interactions, quantum statistics, and thermal fluctuations. We show that operating these thermal machines in the intended regimes, such as a heat engine, refrigerator, thermal accelerator, or heater, would be impossible without such atom-atom correlations. Our results constitute a step forward in the design of conceptually new quantum thermodynamic devices which take advantage of uniquely quantum resources such as quantum coherence, correlations, and entanglement.

Quantum thermal machines (QTM), such as quantum heat engines (QHE), refrigerators, and quantum batteries, are central in the theoretical and experimental development of the emerging field of quantum thermodynamics [1, 2]. Their primary utility is to explore the fundamental laws of thermodynamics in the quantum realm and to demonstrate possible advantages gained by utilising quantum resources. Accordingly, understanding QTM's are expected to play a similar role in the development of quantum technologies as classical heat engines played in fostering scientific advances during the Industrial Revolution. In the past decade, progress in the control over quantum platforms, such as single ions [3, 4], nitrogen vacancy centers [5], and single-atom impurities immersed in an ultra-cold atomic bath [6], have led to the realization of single-particle QHE's. Such single-particle QHE's represent the ultimate limit in the realization of an 'infinitesimal machine' [7].

However, in order to utilize the breadth of quantum resources available, one must move beyond single-particle systems—to engines that utilize interacting many-particle systems. Such QHE's are uniquely positioned to take advantage of quantum resources, such as entanglement [8, 9], correlations [10, 11], or quantum coherence [12, 13], to enhance the performance of classical heat engines [14] or perform entirely new tasks that would be impossible classically [15]. In particular, control over inter-particle interactions allows for the creation of strictly many-body QHE's, [14, 16–19] which have recently been realized in the laboratory [20, 21]. These very recent experimental developments underscore the need for further studies of thermodynamic processes in the context of interacting quantum many-body thermal machines.

Here, we propose a quantum many-body Otto heat engine—as well as related thermal machines such as Otto refrigerator, thermal accelerator, and heater—using a uniform one-dimensional (1D) Bose gas with repulsive contact interactions as the working fluid. In the proposed Otto cycles, the unitary work strokes are driven by a sudden quench of the interaction strength, and we demonstrate how the thermodynamic performance, in particular net work and efficiency, of these many-body QTM's can be calculated through the experimentally measurable atom-atom local pair correlation [22–24]. The atom-atom local correlation, $g^{(2)}(0)$, is described by the second-order Glauber correlation function $g^{(2)}(r)$ at zero interparticle separation (i.e., when $r = 0$, where $r = |x - x'|$ is the distance between the two particles with positions x and x') and characterises the probability of pairs of atoms to be found at the same point, relative to uncorrelated atoms.

The benefits of using the 1D Bose gas as the working fluid in the proposed Otto cycles is that the underlying theoretical model—the Lieb-Liniger model—is exactly solvable in the uniform limit via the Yang-Yang thermodynamic Bethe ansatz (TBA) [25–27], in addition to being experimentally realizable using ultracold atomic gases confined to highly anisotropic traps [28–30]. This offers unique opportunities for gaining physical insights into the performance of such Otto QTM's as a tractable and testable quantum many-body problem. Additionally, the Lieb-Liniger gas has a rich phase diagram spanning several nontrivial regimes [22, 23], from the weakly interacting quasicondensate through to the strongly interacting Tonks-Girardeau regime of fermionization [31, 32]. The atom-atom correlation within these regimes takes on a wide range of values between $0 < g^{(2)}(0) < 2$, depending on the temperature and interaction strength, which aids the operation of the proposed Otto cycles under a variety of conditions. We evaluate the performance of the 1D Bose gas Otto QTM's, but we emphasise that the broad conclusions arrived at here are not limited to the Lieb-Liniger model.

Interaction-driven Otto engine

We start by considering an interaction-driven Otto heat engine cycle with a uniform 1D Bose gas as the working fluid. In a uniform 1D Bose gas, described by the integrable Lieb-Liniger model [25] (see Methods), the interatomic interaction strength χ can be expressed in terms of the harmonic trap frequency $\omega_\perp$ in the tightly confined (transverse) direc-

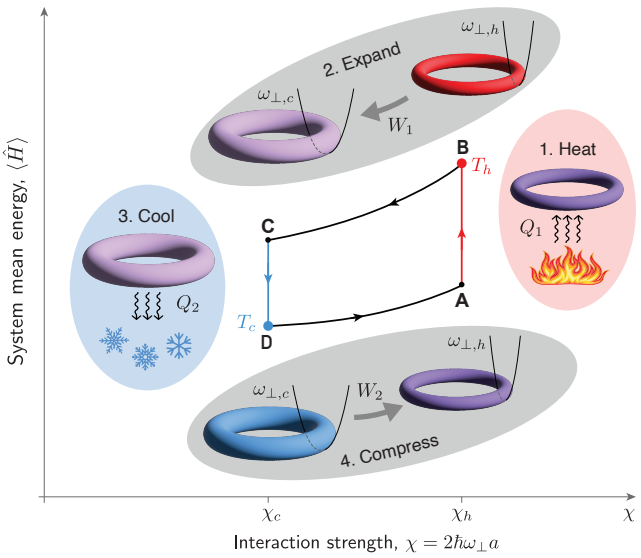

FIG. 1. An interaction-driven quantum many-body Otto cycle, operating between two interaction strengths, χ_c and χ_h. Unitary work strokes (**BC** and **DA**) are shown in black, while non-unitary thermalization strokes (**AB** and **CD**) are color-coded to the cold (blue) and hot (red) reservoirs at temperatures T_c and T_h, respectively.

tion and the 3D s-wave scattering length a_s as $\chi \simeq 2\hbar\omega_\perp a_s$ [33]. Accordingly, changing the interaction strength χ may be achieved by either tuning the external trapping potential that controls the transverse confinement $\omega_\perp$ or by changing the scattering length a_s by means of a magnetic Feshbach resonance [34]. The former option leads to a volume change of the gas (i.e. transverse expansion or compression), and hence can be thought of as analogous to mechanical work in the conventional Otto cycle, however, changing χ via a change of the scattering length leads to identical results, which then justifies our referral to the engine cycle as the Otto cycle regardless of the means of tuning the interaction strength (see Methods). We emphasize, however, that the dynamics of the quantum Otto cycle explored here are strictly longitudinal, with the gas always remaining in its transverse ground state.

The interaction-driven Otto engine cycle, which we thus consider, consists of four strokes (see Fig. 1):

(1) *Thermalization with hot reservoir*, **A**→**B**: the working fluid, consisting of N total atoms at interaction strength χ_h, is connected to a hot (h) reservoir at temperature T_h, where it is left to equilibrate, taking in heat $Q_1 = \langle\hat{H}\rangle_{\mathbf{B}} - \langle\hat{H}\rangle_{\mathbf{A}} > 0$, which is to be partially converted into beneficial work in the subsequent stroke. Here $\hat{H}$ is the system Hamiltonian (see Methods), and $\langle\hat{H}\rangle_{\mathbf{j}}$ is its expectation value, i.e., the total energy of the system, in state $\mathbf{j} = \{\mathbf{A},\mathbf{B},\mathbf{C},\mathbf{D}\}$.

(2) *Unitary expansion,* **B**→**C**: the working fluid, now in a thermal equilibrium state at temperature T_h, is decoupled from the hot reservoir and has its interaction strength quenched from χ_h to $\chi_c < \chi_h$, generating beneficial work $W_1 = \langle\hat{H}\rangle_{\mathbf{C}} - \langle\hat{H}\rangle_{\mathbf{B}} < 0$ done by the fluid.

(3) *Thermalization with cold reservoir*, **C**→**D**: the working fluid is connected to a cold (c) reservoir at temperature $T_c < T_h$ and allowed to equilibrate at constant interaction strength χ_c while dumping energy in the form of heat $Q_2 = \langle\hat{H}\rangle_{\mathbf{D}} - \langle\hat{H}\rangle_{\mathbf{C}} < 0$ into the cold reservoir.

(4) *Unitary compression*, **D**→**A**: disconnected from the cold reservoir, the working fluid has its interaction strength quenched from $\chi_c \to \chi_h$, with work $W_2 = \langle\hat{H}\rangle_{\mathbf{A}} - \langle\hat{H}\rangle_{\mathbf{D}} > 0$ done on the fluid, and the system returning to the initial state of the overall cycle.

Such an engine cycle generates net beneficial work (done by the fluid) if the total work $W = W_1 + W_2 < 0$, i.e., if $|W_1| > W_2$ (or $Q_1 > |Q_2|$), with efficiency $\eta = -W/Q_1 = 1 - |Q_2|/Q_1$, where we used the conservation of energy $W + Q = 0$, with $Q = Q_1 + Q_2$ being the total heat [35].

Work from second-order Glauber correlations

In this work, we specifically consider a sudden or instantaneous quench of the interaction strength χ in the unitary strokes (2) and (4). (For a discussion of "instantaneity" of the sudden quench, see Methods). Under a sudden interaction quench, the initial (i) and final (f) expectation values over field operators in the system Hamiltonian, i.e., the expectation values before and after the quench, remain unchanged as the system did not have sufficient time to evolve into a new state. Hence, the only contribution to the difference in total energy before and after the quench, $\langle\hat{H}\rangle_f - \langle\hat{H}\rangle_i$, comes from the difference between the interaction terms, $\frac{1}{2}\chi_f \int dz \langle\hat{\Psi}^\dagger\hat{\Psi}^\dagger\hat{\Psi}\hat{\Psi}\rangle_f - \frac{1}{2}\chi_i \int dz \langle\hat{\Psi}^\dagger\hat{\Psi}^\dagger\hat{\Psi}\hat{\Psi}\rangle_i$, where $\langle\hat{\Psi}^\dagger\hat{\Psi}^\dagger\hat{\Psi}\hat{\Psi}\rangle_f = \langle\hat{\Psi}^\dagger\hat{\Psi}^\dagger\hat{\Psi}\hat{\Psi}\rangle_i$ in a sudden quench, and $\hat{\Psi}^\dagger(z)$ and $\hat{\Psi}(z)$ represent the field creation and annihilation operators. Accordingly, the energy difference can be expressed as $\langle\hat{H}\rangle_f - \langle\hat{H}\rangle_i = \frac{1}{2}(\chi_f - \chi_i)\overline{G_i^{(2)}}$, where we have defined the total (integrated) second-order correlation of the thermal equilibrium state $\overline{G_i^{(2)}} = \int dz \langle\hat{\Psi}^\dagger\hat{\Psi}^\dagger\hat{\Psi}\hat{\Psi}\rangle_i$ [23].

Identifying the i and f states as points **B** (hot, h) and **C**, or as **D** (cold, c) and **A** in the digram of Fig. 1, the net work of the Otto engine can be expressed as

$$W = -\frac{1}{2}(\chi_h - \chi_c)\left(\overline{G_h^{(2)}} - \overline{G_c^{(2)}}\right). \tag{1}$$

Likewise, the efficiency of the engine may be expressed as

$$\eta = 1 - \frac{\langle\hat{H}\rangle_h - \langle\hat{H}\rangle_c - \frac{1}{2}(\chi_h - \chi_c)\,\overline{G_h^{(2)}}}{\langle\hat{H}\rangle_h - \langle\hat{H}\rangle_c - \frac{1}{2}(\chi_h - \chi_c)\,\overline{G_c^{(2)}}}. \tag{2}$$

These equations allow for investigation of the interaction-driven Otto engine under a sudden quench protocol through solely the equilibrium properties of the gas, as all expectation values involved are with respect to h (**B**) or c (**D**) states.

Finite-temperature uniform 1D Bose gases have no phase transition to a true Bose-Einstein condensate in the thermo-

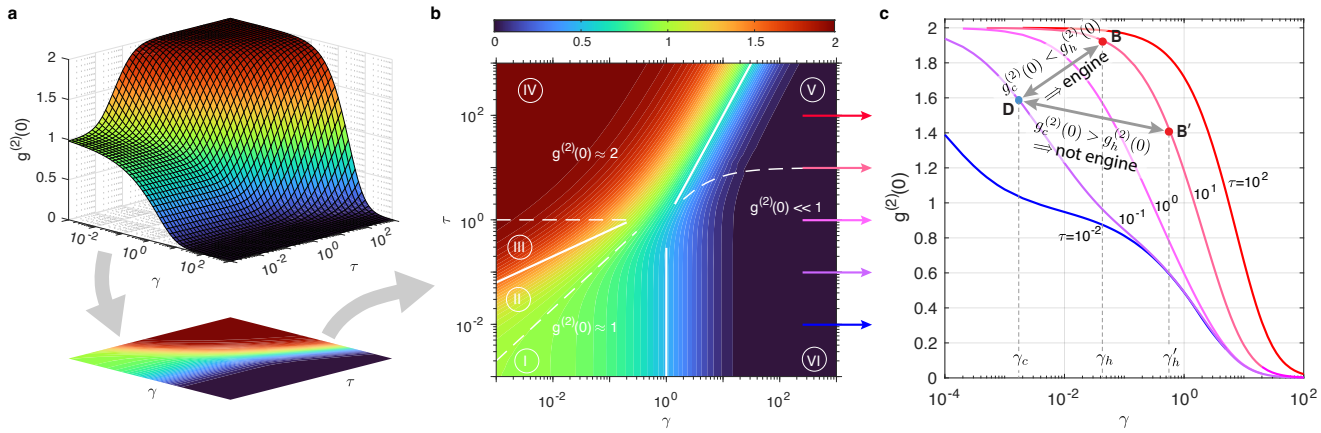

FIG. 2. Atom-atom correlations, described by Glauber's $g^{(2)}(0)$ correlation function, for the uniform 1D Bose gas evaluated using the exact Yang-Yang TBA [22, 26]. Panel **a** shows $g^{(2)}(0)$ as a function of the dimensionless interaction strength, γ, and temperature, τ. In panel **b**, this is translated into a contour diagram, in which we also show the crossover boundaries (white solid and dashed lines) between the different asymptotic analytic regimes [22]. Panel (**c**) shows line plots of $g^{(2)}(0)$ vs γ, at different fixed values of τ, together with two possible choices, **D-B** or **D-B′**, of the thermal equilibrium operating points of the Otto cycle from Fig. 1; as we see, according to Eq. (1), operating the Otto cycle as an engine (with $W < 0$) can be achieved between the points **D-B** ($\gamma_c \longleftrightarrow \gamma_h$), where $g_c^{(2)}(0) < g_h^{(2)}(0)$, but not between **D-B′** ($\gamma_c \longleftrightarrow \gamma_h'$), where $g_c^{(2)}(0) > g_h^{(2)}(0)$ due to the stronger interaction quench, even though the temperature at **D** is still lower than at **B′**.

dynamic limit, unlike Bose-Einstein condensation in three dimensions [36]. However, there still exists a rich crossover phase diagram of different regimes that can be characterised by the normalized local (same-point) atom-atom pair correlation function $g^{(2)}(0)$ (see Methods and Refs. [22]). The pair correlation function is a thermodynamic quantity that can be calculated from the exact TBA, as well as using approximate analytic methods [22], and is shown in Figs. 2 **a** and **b**. This function, and hence the different regimes of the uniform 1D Bose gas, can be parameterized by dimensionless interaction strength, $\gamma = m\chi/\hbar^2\rho$, and dimensionless temperature, $\tau = 2mk_BT/\hbar^2\rho^2$, where m is the boson mass and $\rho = N/L$ is the 1D density for N atoms in a system of length L.

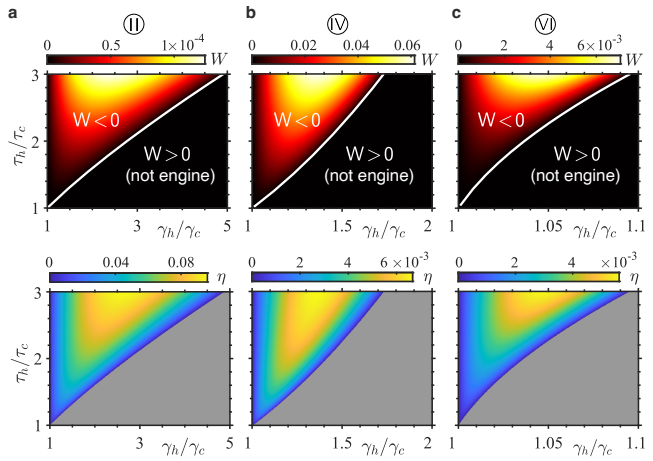

FIG. 3. Performance of the interaction-driven quantum Otto engine. Columns, **a**, **b**, and **c**, demonstrate net work, W, and efficiency, η, as a function of the ratio of interaction strength, γ_h/γ_c, and temperature, τ_h/τ_c, between the hot (h) and cold (c) thermal equilibrium states. The example of panel **a** is for $\gamma_c = 10^{-3}$ and $\tau_c = 10^{-2}$, where γ_h/γ_c and τ_h/τ_c explores the parameter range within the region II of the equilibrium regimes diagram of Fig. 2**b**. Similarly, panel **b** explores region IV, with $\gamma_c = 1$ and $\tau = 10$, whereas panel **c** explores region VI, with $\gamma_c = 10$ and $\tau = 1$.

For a uniform 1D Bose gas, the total correlation in the hot or cold thermal equilibrium state may be expressed as $\overline{G_{h\mathbf{c}}^{(2)}} = N\rho g_{h\mathbf{c}}^{(2)}(0)$ (see Methods). Combining this with Eq. (1), the net work per particle can be expressed as

$$\frac{W}{N} = -\frac{\hbar^2\rho^2}{2m}(\gamma_h - \gamma_c)\left(g_h^{(2)}(0) - g_c^{(2)}(0)\right), \qquad (3)$$

i.e., the net work is directly proportional to the difference between atom-atom correlations of the 1D Bose gas in the hot and cold thermal equilibrium states. This simple relationship between thermodynamic work and Glauber second-order correlation function represents one of the key results of this work.

From Eq. (3), and given that γ_h is always larger than γ_c, we see that if the local pair correlations did not depend on the respective interaction strengths and temperatures, i.e. if they were the same, $g_h^{(2)}(0) = g_c^{(2)}(0)$, then the net work per particle would vanish. We therefore conclude that extracting net work ($W < 0$) from this Otto cycle, and hence operating it as a heat engine, can only be enabled by atom-atom correlations; more specifically, the only way to extract net work is to have $g_h^{(2)}(0) > g_c^{(2)}(0)$ (see Figs. 2 **c**).

Net work, Eq. (3), and efficiency, Eq. (2), of this quantum Otto engine, calculated for simplicity using analytic approximations to the atom-atom correlation function and total energy [22], are shown in Fig. 3 as a function of the ratio

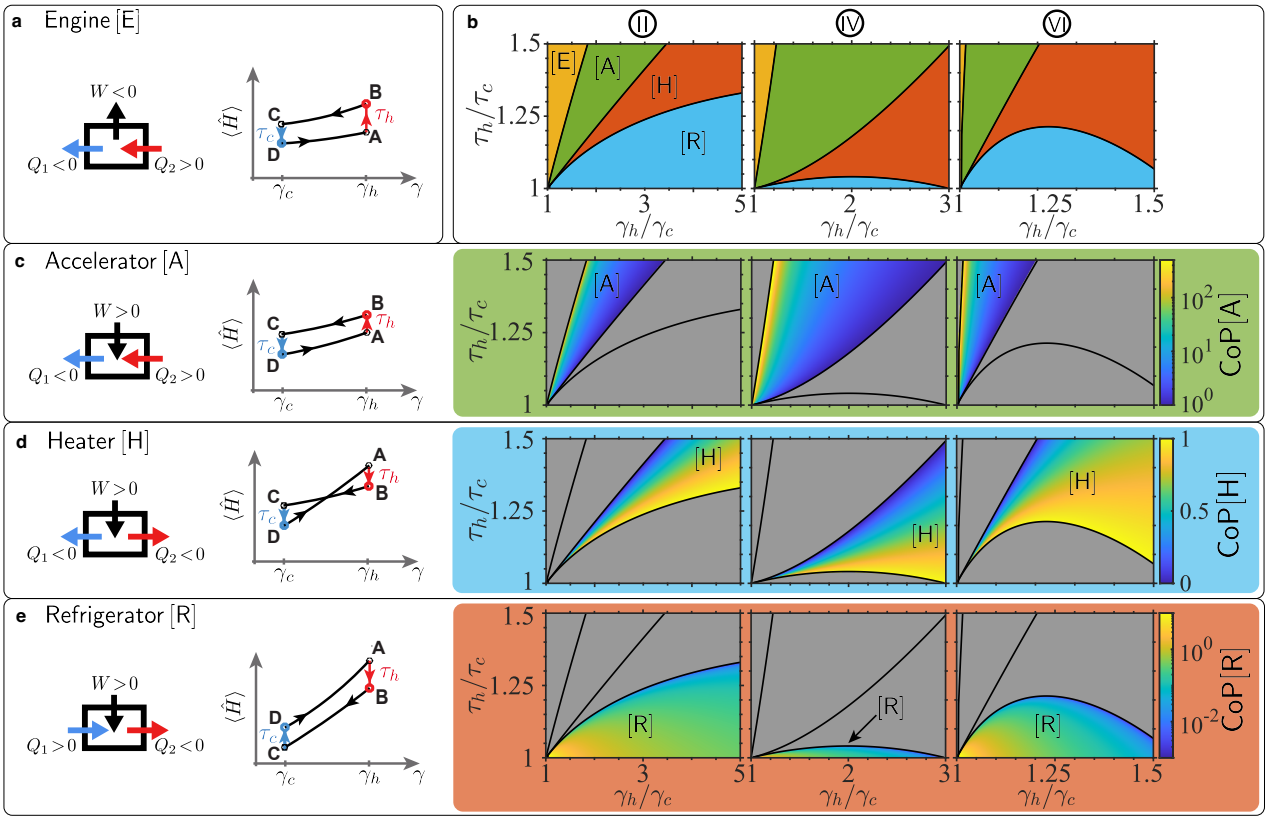

FIG. 4. Performance of the interaction-driven quantum Otto cycles in the accelerator ([A]), heater ([H]), and refrigerator ([R]) regimes. An energy flow diagram (left) for the interaction-driven Otto engine ([E]) is shown for comparison in panel **a** alongside a simplified version of the cycle diagram (right), originally depicted in Fig. 1. Panel **b** shows a simplified layout of how the operating regimes of different QTM's depend on the ratio of interaction strengths, γ_h/γ_c, and temperatures, τ_h/τ_c, of the hot and cold thermal states in same the three asymptotic regimes as in Fig. 3. The energy flow and cycle diagrams for the accelerator QTM are illustrated in panel **c**, where we additionally plot its coefficient of performance, CoP[A] (see text), in the chosen asymptotic parameter regimes. Likewise, in panels **d** and **e** we show the energy flow, cycle diagrams, and coefficients of performance for the heater and refrigerator regimes, respectively.

of interaction strengths, γ_h/γ_c, and temperatures, τ_h/τ_c, for three of the six asymptotic regimes (for results outside of the regimes of analytic approximation, see Methods). Notably, in this Otto engine cycle, for any fixed value of the temperature ratio, the interaction strength quench corresponding to maximum net work is approximately the same as that providing maximum efficiency; this occurs as, to first order, the heat intake Q_1 varies slowly with γ_h/γ_c, meaning $\eta \propto W$ (see Methods). The observed increase of net work and efficiency in all regimes under large temperature ratio may be attributed to the fact that the local correlation of the hot thermal state in Eq. (3) is always a monotonically increasing function of τ. However, as the correlation function is also monotonically decreasing under γ_h, this results in no extractable net work under sufficiently large interaction strength ratios for any given temperature ratio.

At a glance, one may conclude that the net work, which is enabled through the $g^{(2)}(0)$ correlation function, is maximized under the largest possible difference in correlation function, i.e. $g_h^{(2)}(0) - g_c^{(2)}(0) \simeq 2$. However, to achieve this, while also guaranteeing that $\gamma_h > \gamma_c$, would require an unrealistically high (from practical point of view) temperature ratio to operate between regimes VI and IV, shown in Fig. 2. Rather, we observe that, while the $g^{(2)}(0)$ correlation function is responsible for enabling operation as a heat engine, the *magnitude* of net work is governed more strongly by the difference in the interaction strengths, $\gamma_h - \gamma_c$, which is unrestricted. Consequently, it is in the weakly interacting ($\gamma \ll 1$) region II that we observe the lowest magnitude of net work (see Fig. 3**a**), where $\gamma_h - \gamma_c$ is very small. In comparison, the magnitude of net work is largest in regime IV, shown in Fig. 3**b**, where $\gamma \sim 1$ and hence the difference $\gamma_h - \gamma_c$ can also be on the order of one. The same considerations apply to the strongly interacting ($\gamma \gg 1$) regime VI, where one can operate under the largest magnitudes of interaction strengths, however, in this regime the net work is diminished due to the vanishing of correlation itself ($g^{(2)} \ll 1$) due to the effect of fermionization. In contrast to these observations, the efficiency of the engine, Eq. (2), is inversely dependent on the total energy of the thermal states, which is minimal in the weakly interacting low temperature regime II, which thus has the largest efficiency. Further, we note that the effi-

ciencies presented in Fig. 3, while of low magnitude, are not significantly reduced when compared to the corresponding reversible engine cycle results (see Methods).

Interaction-driven Otto accelerator, heater, and refrigerator

Glauber's $g^{(2)}(0)$ correlation function for the 1D Bose gas is inherently dependent on the interaction strength and temperature [22]. This implies that the condition for the Otto cycle to operate as a heat engine, $g_c^{(2)}(0) < g_h^{(2)}(0)$, where $\gamma_c < \gamma_h$, cannot hold under large quenches of interaction strength from γ_c to γ_h as the gas becomes increasingly fermionized (i.e., $g_h^{(2)}(0) \to 0$) in the limit $\gamma \to \infty$ [31]. However, beyond the heat engine operation regime, a further three QTM's are thermodynamically allowed [37]: namely, accelerator [A], heater [H], and refrigerator [R]. For these QTM's, one may define a coefficient of performance (CoP) according to the following principle [38]:

$$\mathrm{CoP[QTM]} = \frac{\text{benefit of operation}}{\text{cost of operation}}. \tag{4}$$

In the left two columns of Fig. 4, we show the simplified schematics of these additional QTM's compared to the heat engine from Fig. 1, which we repeat here in **a** for comparison; in panel **b** we show the operating boundaries of these different QTM's. Finally, in the color coded right panels in **c**–**e**, we show the magnitudes of the respective CoP's, which we now defined and discuss in greater detail.

Accelerator [A].—The conditions of operating the Otto cycle as a thermal accelerator are given by: $W > 0$, $Q_1 > 0$, $Q_2 < 0$, where $W = 0$ defines the border between the heat engine and the accelerator. This QTM [37] enhances the natural flow of heat, taken into the working fluid from the hot reservoir, Q_1, and transferred to the cold reservoir, Q_2, by investing net mechanical work, W, in the process. According to Eq. (4), its CoP is given by:

$$\mathrm{CoP[A]} = -\frac{Q_2}{W} = 1 + \frac{Q_1}{W} > 1, \tag{5}$$

where,

$$Q_2 = -\langle \hat{H} \rangle_h + \langle \hat{H} \rangle_c + \frac{N\hbar^2\rho^2}{2m}(\gamma_h - \gamma_c) g_h^{(2)}(0), \tag{6}$$

$$Q_1 = \langle \hat{H} \rangle_h - \langle \hat{H} \rangle_c - \frac{N\hbar^2\rho^2}{2m}(\gamma_h - \gamma_c) g_c^{(2)}(0). \tag{7}$$

The magnitude of CoP[A] is shown Fig. 4 **c**, where we note that, at the border between [E] and [A], the coefficient of performance diverges due to its inverse dependence on W. Operation of this QTM, enabled through $g_h^{(2)}(0) < g_c^{(2)}(0)$, additionally requires that the work in and out, which are proportional to $g_c^{(2)}(0)$ and $g_h^{(2)}(0)$, respectively, remain small in comparison to the energy gap between the hot and cold thermal states, as shown in the cycle diagram in Fig. 4 **c**. This is in direct contrast with the two further QTM's described below.

Heater [H].—Operating the Otto cycle in the heater regime requires: $W > 0, Q_1 < 0$, $Q_2 < 0$, and is shown schematically in Fig. 4 **d**. This QTM utilizes mechanical work to heat up both hot and cold thermal reservoirs. The border with the accelerator regime is defined by $Q_1 = 0$. This condition depends on the competition between $\langle \hat{H} \rangle_h$ and $\gamma_h g_c^{(2)}(0)$, with all other terms fixed by γ_c and τ_c, defining the cold thermal state. However, we note that for a fixed temperature ratio, τ_h/τ_c, an arbitrarily large interaction strength quench inevitably incurs operation as a heater (see Methods).

The CoP for the heater regime, if one considers the benefit of operation to be heating of *both* reservoirs then, due to the conservation of energy, is trivially $\mathrm{CoP[H]} = -Q/W = 1$. Instead, in Fig. 4 **d**, we define the benefit of operation to be the heating of the hot reservoir , thus

$$\mathrm{CoP[H]} = -\frac{Q_1}{W} = 1 - \frac{|Q_2|}{W} < 1. \tag{8}$$

One may alternatively define the benefit of the heater as heating the cold reservoir,

$$\mathrm{CoP[H]}' = -\frac{Q_2}{W} = 1 - \mathrm{CoP[H]} < 1. \tag{9}$$

Both definitions of $\mathrm{CoP[H]}$, however, are limited by energy conservation to be less than or equal to 1.

Refrigerator [R].—The conditions of operating the Otto cycle as a refrigerator are: $W > 0$, $Q_1 < 0$, $Q_2 > 0$. The purpose of this thermal machine is to cool down the cold reservoir by extracting heat and dumping it into the hot reservoir, with the aid mechanical work done by the working fluid. The boundary between [H] and [R] is defined by $Q_2 = 0$. The CoP for the refrigerator is given by [38]

$$\mathrm{CoP[R]} = \frac{Q_2}{W} = \frac{|Q_1|}{W} - 1, \tag{10}$$

and is shown in Fig. 4 **e**; it diverges in the limit of infinitesimal quenches in both interaction strength and temperature due to the rapid convergence of $W \to 0$, which is faster than that of $Q_1 \to 0$ (see Methods).

The conditions on $g_h^{(2)}(0)$ and $g_c^{(2)}(0)$ for operating in this regime run directly counter to operation as an accelerator. For refrigeration, the correlation functions must remain large enough that the work in and out exceed the energy gap between the two thermal states, as shown in the cycle diagram in Fig. 4 **e**. However, as noted above, large interaction strength quenches inevitably reduce the work out as $g_h^{(2)}(0)$ reduces rapidly for large γ_h, thus incurring operation as a heater for any given temperature ratio. This implies that the refrigerator occurs only over a finite parameter region, most clearly visible in regimes IV and VI of Fig. 4 **e**.

Summary and outlook

We have proposed a sudden interaction-quench Otto cycle operating in a quantum many-body regime using a repulsive

1D Bose gas as a working fluid. Extracting net work from such an engine was shown to be enabled by atom-atom correlations. Such correlations are characterized by Glauber's second-order correlation function, $g^{(2)}(0)$, which in fact is a thermodynamic quantity that can be calculated from the exact thermodynamic Bethe ansatz solution through application of the Hellmann-Feynman theorem to the Helmholtz free energy [22]. Further, we have investigated in detail the various operational regimes of this Otto cycle, including the thermal accelerator, heater, and refrigerator cycles, defining and examining their coefficients of performance.

Though our specific results for the net work and the efficiency were calculated for a uniform 1D Bose as an example, the broad conclusions arrived at here on the basis of equations (1) and (2) are applicable to any other many-body system with short-range contact interactions and should aid the tests of quantum thermodynamic concepts and realization of novel QTMs in laboratory settings.

This work was supported through Australian Research Council Discovery Project Grant No. DP190101515.

[1] S. Vinjanampathy and J. Anders, Quantum thermodynamics, Contemporary Physics **57**, 545 (2016).

[2] R. Kosloff and A. Levy, Quantum Heat Engines and Refrigerators: Continuous Devices, Annual Review of Physical Chemistry **65**, 365 (2014).

[3] J. Roßnagel, S. T. Dawkins, K. N. Tolazzi, O. Abah, E. Lutz, F. Schmidt-Kaler, and K. Singer, A single-atom heat engine, Science **352**, 325 (2016).

[4] D. von Lindenfels, O. Gräb, C. T. Schmiegelow, V. Kaushal, J. Schulz, M. T. Mitchison, J. Goold, F. Schmidt-Kaler, and U. G. Poschinger, Spin Heat Engine Coupled to a Harmonic-Oscillator Flywheel, Phys. Rev. Lett. **123**, 080602 (2019).

[5] J. Klatzow, J. N. Becker, P. M. Ledingham, C. Weinzetl, K. T. Kaczmarek, D. J. Saunders, J. Nunn, I. A. Walmsley, R. Uzdin, and E. Poem, Experimental Demonstration of Quantum Effects in the Operation of Microscopic Heat Engines, Phys. Rev. Lett. **122**, 110601 (2019).

[6] Q. Bouton, J. Nettersheim, S. Burgardt, D. Adam, E. Lutz, and A. Widera, A quantum heat engine driven by atomic collisions, Nature Communications **12**, 2063 (2021).

[7] R. Feynman, There's plenty of room at the bottom, in *Feynman and computation* (CRC Press, Boca Raton, Florida, United States, 2018) pp. 63–76.

[8] F. G. Brandao and M. B. Plenio, Entanglement theory and the second law of thermodynamics, Nature Physics **4**, 873 (2008).

[9] K. Funo, Y. Watanabe, and M. Ueda, Thermodynamic work gain from entanglement, Phys. Rev. A **88**, 052319 (2013).

[10] J. Oppenheim, M. Horodecki, P. Horodecki, and R. Horodecki, Thermodynamical Approach to Quantifying Quantum Correlations, Phys. Rev. Lett. **89**, 180402 (2002).

[11] M. Perarnau-Llobet, K. V. Hovhannisyan, M. Huber, P. Skrzypczyk, N. Brunner, and A. Acín, Extractable Work from Correlations, Phys. Rev. X **5**, 041011 (2015).

[12] V. Narasimhachar and G. Gour, Low-temperature thermodynamics with quantum coherence, Nature communications **6**, 7689 (2015).

[13] K. Korzekwa, M. Lostaglio, J. Oppenheim, and D. Jennings, The extraction of work from quantum coherence, New Journal of Physics **18**, 023045 (2016).

[14] J. Jaramillo, M. Beau, and A. del Campo, Quantum supremacy of many-particle thermal machines, New Journal of Physics **18**, 075019 (2016).

[15] N. Yunger Halpern, C. D. White, S. Gopalakrishnan, and G. Refael, Quantum engine based on many-body localization, Phys. Rev. B **99**, 024203 (2019).

[16] M. Beau, J. Jaramillo, and A. Del Campo, Scaling-Up Quantum Heat Engines Efficiently via Shortcuts to Adiabaticity, Entropy **18**, 10.3390/e18050168 (2016).

[17] J. Li, T. Fogarty, S. Campbell, X. Chen, and T. Busch, An efficient nonlinear Feshbach engine, New Journal of Physics **20**, 015005 (2018).

[18] Y.-Y. Chen, G. Watanabe, Y.-C. Yu, X.-W. Guan, and A. del Campo, An interaction-driven many-particle quantum heat engine and its universal behavior, npj Quantum Information **5**, 88 (2019).

[19] T. Keller, T. Fogarty, J. Li, and T. Busch, Feshbach engine in the Thomas-Fermi regime, Physical Review Research **2**, 033335 (2020).

[20] J. Koch, K. Menon, E. Cuestas, S. Barbosa, E. Lutz, T. Fogarty, T. Busch, and A. Widera, A quantum engine in the BEC–BCS crossover, Nature **621**, 723 (2023).

[21] E. Q. Simmons, R. Sajjad, K. Keithley, H. Mas, J. L. Tanlimco, E. Nolasco-Martinez, Y. Bai, G. H. Fredrickson, and D. M. Weld, Thermodynamic engine with a quantum degenerate working fluid, Phys. Rev. Res. **5**, L042009 (2023).

[22] K. V. Kheruntsyan, D. M. Gangardt, P. D. Drummond, and G. V. Shlyapnikov, Pair Correlations in a Finite-Temperature 1D Bose Gas, Phys. Rev. Lett. **91**, 040403 (2003).

[23] K. V. Kheruntsyan, D. M. Gangardt, P. D. Drummond, and G. V. Shlyapnikov, Finite-temperature correlations and density profiles of an inhomogeneous interacting one-dimensional Bose gas, Phys. Rev. A **71**, 053615 (2005).

[24] T. Kinoshita, T. Wenger, and D. S. Weiss, Local Pair Correlations in One-Dimensional Bose Gases, Phys. Rev. Lett. **95**, 190406 (2005).

[25] E. H. Lieb and W. Liniger, Exact Analysis of an Interacting Bose Gas. I. The General Solution and the Ground State, Phys. Rev. **130**, 1605 (1963).

[26] C. N. Yang and C. P. Yang, Thermodynamics of a One-Dimensional System of Bosons with Repulsive Delta-Function Interaction, Journal of Mathematical Physics **10**, 1115 (1969).

[27] V. E. Korepin, N. M. Bogoliubov, and A. G. Izergin, *Quantum Inverse Scattering Method and Correlation Functions*, Cambridge Monographs on Mathematical Physics (Cambridge University Press, Cambridge, United Kingdom, 1993).

[28] A. Görlitz, J. M. Vogels, A. E. Leanhardt, C. Raman, T. L. Gustavson, J. R. Abo-Shaeer, A. P. Chikkatur, S. Gupta, S. Inouye, T. Rosenband, and W. Ketterle, Realization of Bose-Einstein Condensates in Lower Dimensions, Phys. Rev. Lett. **87**, 130402 (2001).

[29] M. Greiner, I. Bloch, O. Mandel, T. W. Hänsch, and T. Esslinger, Exploring Phase Coherence in a 2D Lattice of Bose-Einstein Condensates, Phys. Rev. Lett. **87**, 160405 (2001).

[30] F. Schreck, L. Khaykovich, K. L. Corwin, G. Ferrari, T. Bourdel, J. Cubizolles, and C. Salomon, Quasipure Bose-Einstein Condensate Immersed in a Fermi Sea, Phys. Rev. Lett. **87**, 080403 (2001).

[31] M. Girardeau, Relationship between Systems of Impenetrable

Bosons and Fermions in One Dimension, Journal of Mathematical Physics **1**, 516 (1960).
[32] T. Kinoshita, T. Wenger, and D. S. Weiss, Observation of a One-Dimensional Tonks-Girardeau Gas, Science **305**, 1125 (2004).
[33] M. Olshanii, Atomic Scattering in the Presence of an External Confinement and a Gas of Impenetrable Bosons, Phys. Rev. Lett. **81**, 938 (1998).
[34] C. Chin, R. Grimm, P. Julienne, and E. Tiesinga, Feshbach resonances in ultracold gases, Rev. Mod. Phys. **82**, 1225 (2010).
[35] H. B. Callen, *Thermodynamics and an introduction to thermostatistics*, 2nd ed. (John Wiley & Sons, Hoboken, New Jersey, 1985).
[36] C. J. Pethick and H. Smith, *Bose–Einstein condensation in dilute gases* (Cambridge university press, Cambridge, United Kingdom, 2008).
[37] L. Buffoni, A. Solfanelli, P. Verrucchi, A. Cuccoli, and M. Campisi, Quantum measurement cooling, Phys. Rev. Lett. **122**, 070603 (2019).
[38] D. V. Schroeder, *An introduction to thermal physics* (Oxford University Press, Oxford, 2020).
[39] R. Kosloff, A quantum mechanical open system as a model of a heat engine, The Journal of Chemical Physics **80**, 1625 (1984).
[40] R. Kosloff and Y. Rezek, The Quantum Harmonic Otto Cycle, Entropy **19**, 10.3390/e19040136 (2017).
[41] Y. Zheng and D. Poletti, Work and efficiency of quantum Otto cycles in power-law trapping potentials, Phys. Rev. E **90**, 012145 (2014).
[42] G. Watanabe, B. P. Venkatesh, P. Talkner, and A. del Campo, Quantum Performance of Thermal Machines over Many Cycles, Phys. Rev. Lett. **118**, 050601 (2017).
[43] O. Abah and E. Lutz, Energy efficient quantum machines, Europhysics Letters **118**, 40005 (2017).
[44] N. M. Myers, F. J. Peña, O. Negrete, P. Vargas, G. D. Chiara, and S. Deffner, Boosting engine performance with Bose–Einstein condensation, New Journal of Physics **24**, 025001 (2022).
[45] C. Mora and Y. Castin, Extension of Bogoliubov theory to quasicondensates, Phys. Rev. A **67**, 053615 (2003).
[46] A. G. Sykes, D. M. Gangardt, M. J. Davis, K. Viering, M. G. Raizen, and K. V. Kheruntsyan, Spatial nonlocal pair correlations in a repulsive 1d bose gas, Phys. Rev. Lett. **100**, 160406 (2008).
[47] G. D. Rosi, R. Rota, G. E. Astrakharchik, and J. Boronat, Hole-induced anomaly in the thermodynamic behavior of a one-dimensional Bose gas, SciPost Phys. **13**, 035 (2022).
[48] B. Yang, Y.-Y. Chen, Y.-G. Zheng, H. Sun, H.-N. Dai, X.-W. Guan, Z.-S. Yuan, and J.-W. Pan, Quantum criticality and the Tomonaga-Luttinger liquid in one-dimensional Bose gases, Phys. Rev. Lett. **119**, 165701 (2017).

Methods

The Lieb-Liniger model for the 1D Bose gas.—The uniform 1D Bose gas with repulsive contact interactions [25] is described by the second-quantized Hamiltonian

$$\begin{aligned}\hat{H} &= \hat{H}^{kin} + \hat{H}^{int} \\ &= -\frac{\hbar^2}{2m}\int dz \hat{\Psi}^\dagger \frac{\partial^2}{\partial z^2}\hat{\Psi} + \frac{\chi}{2}\int dz \hat{\Psi}^\dagger\hat{\Psi}^\dagger\hat{\Psi}\hat{\Psi},\end{aligned} \tag{11}$$

where m is the atomic mass, χ is the strength of the contact interactions (see main text), and $\hat{\Psi}^\dagger(z)$ and $\hat{\Psi}(z)$ are the bosonic field creation and annihilation operators, respectively. We additionally highlight the separation of the Lieb-Liniger Hamiltonian into its kinetic energy, $\hat{H}^{kin}$, and interaction energy, $\hat{H}^{int}$, components, to be referred to later.

Ground state solutions to this integrable model are dependent only on a single dimensionless interaction strength, $\gamma = m\chi/\hbar^2\rho$, where $\rho = N/L$ is the linear density for N particles in a system of size L. Finite temperature solutions, on the other hand, can be obtained using the Yang-Yang thermodynamic Bethe ansatz (TBA) [26], and can be parametrised by an additional dimensional parameter, the dimensionless temperature $\tau = 2mk_BT/\hbar^2\rho^2$ [22].

Instantaneity of the sudden quench.—Realistically, a sudden quench of interaction strength from $\chi_{h\mathfrak{c}}$ to $\chi_{c(h)}$ would still occur over a finite duration Δt. The "instantaneity" of the quench utilized in the main text refers to the assumption that Δt is much shorter than the characteristic time scale for longitudinal dynamics, i.e. that $\Delta t \ll ml_{\text{cor}}^2/\hbar$, where l_{cor} is the characteristic short-range correlation length in the system, given, respectively, by: the healing length $l_h = \hbar/\sqrt{m\chi\rho}$ in regimes I and II; thermal phase coherence length $l_\phi = \hbar^2\rho/mk_BT$ in regime III; thermal de Broglie wavelength $\lambda_T = \sqrt{2\pi\hbar^2/mk_BT}$ in regime IV; absolute value of the 1D scattering length $|a_{1D}| = 2\hbar^2/m\chi$ in the regime of high-temperature fermionization V; and the Fermi wavelength $\lambda_F = 2/\rho$ in the Tonks-Girardeau regime of low-temperature fermionization VI. Thus, it is with respect to the *longitudinal* dynamics that we refer to our quench as sudden. With respect to the *transverse* dynamics, on the other hand, we are assuming that Δt is sufficiently long ($\Delta t \gg 2\pi/\omega_\perp$) compared to the characteristic transverse timescale, $2\pi/\omega_\perp$, governed by the transverse harmonic trap frequency $\omega_\perp$ [33]. As a result, the quench would retain the system in the transverse ground state, and hence would not compromise the 1D character of the system. As such, the work done on (or by) the system during the unitary strokes can be regarded as transversely quasistatic.

Transverse Otto cycle.—For a magnetically trapped ultracold 1D Bose gas, the work done via transverse compression and expansion is ultimately magnetic: it is done by the magnetic field on the atomic dipole moments when $\omega_\perp$ is increased, or vice versa – by the atomic dipole moments on the magnetic field when $\omega_\perp$ is decreased. Alternatively, the change in the interaction strength χ is implemented through control over the s-wave scattering length a_s via a magnetic

Feshbach resonance [34], in which case the nature of the work is still magnetic.

We use the term Otto cycle in the same sense as used to describe, e.g., a harmonic oscillator Otto engine [6, 17, 18, 20, 39–44], wherein the harmonic oscillator frequency (rather than the volume of the system) is fixed as an external parameter during the thermalization strokes. In our case, it is the interaction strength that is fixed, which itself is proportional to the transverse harmonic confinement frequency of the 1D Bose gas.

Glauber's second order correlation function.— The two-point correlation function may be generally defined through

$$g^{(2)}(z,z') = \frac{\langle \hat{\Psi}^\dagger(z)\hat{\Psi}^\dagger(z')\hat{\Psi}(z')\hat{\Psi}(z)\rangle}{\rho(z)\rho(z')}. \tag{12}$$

For a uniform (translationally invariant) system with $\rho(z') = \rho(z) = \rho$, this $g^{(2)}(z,z')$ depends only on the relative distance $|z-z'|$, i.e. $g^{(2)}(z,z') = g^{(2)}(|z-z'|)$. If one is interested in the same point ($z = z'$) correlation function, as utilized in the main text for calculation of the net work and efficiency of the quantum Otto cycle, this in turn becomes $g^{(2)}(0)$.

The 1D Bose gas can be characterized by six distinct asymptotic regimes defined through the same-point correlation function [22], as shown in Fig. 2. The weakly interacting ($\gamma \ll 1$), low temperature quasicondensate regime can be treated using the Bogoliubov theory for quasicondensates [45], and is characterised by suppressed density fluctuations, but fluctuating phase. This may be subdivided into regions dominated by quantum (I) and thermal (II) fluctuations [22]. At higher temperatures, the gas becomes nearly ideal, and can be treated using perturbation theory with respect to γ [22, 46]. This asymptotic region may in turn be subdivided into quantum degenerate (III) and non-degenerate (IV) regimes. Finally, in the strongly interacting regime ($\gamma \gg 1$), where the Fermi-Bose gas mapping applies, the 1D Bose gas can be well approximated by a nearly ideal Fermi gas, and can be treated using pertubation theory with respect to $1/\gamma$ [22, 46]. This regime can be further subdivided into two regions corresponding to high-temperature (V) and low-temperature (VI) fermionization.

In each of these asymptotic regimes, the pair correlation function $g^{(2)}$ can be derived in closed approximate analytic form, where we additionally define the boundary of these regimes in terms of γ and τ:

$$\text{I}: \; g^{(2)} \simeq 1 - \frac{2}{\pi}\gamma^{1/2} + \frac{\pi\,\tau^2}{24\,\gamma^{3/2}}, \quad [\tau/2 \ll \gamma \ll 1], \tag{13}$$

$$\text{II}: \; g^{(2)} \simeq 1 + \frac{\tau}{2\sqrt{\gamma}}, \quad [2\gamma \ll \tau \ll 2\sqrt{\gamma}], \tag{14}$$

$$\text{III}: \; g^{(2)} \simeq 2 - \frac{4\gamma}{\tau^2}, \quad [2\sqrt{\gamma} \ll \tau \ll 1], \tag{15}$$

$$\text{IV}: \; g^{(2)} \simeq 2 - \gamma\sqrt{\frac{2\pi}{\tau}}, \quad [\tau \gg \max\{1, \gamma^2\}], \tag{16}$$

$$\text{V}: \; g^{(2)} \simeq \frac{2\tau}{\gamma^2}, \quad \left[\frac{\pi^2}{(1+2/\gamma)^2} \ll \tau \ll \gamma^2\right], \tag{17}$$

$$\text{VI}: \; g^{(2)} \simeq \frac{4\pi^2}{3\gamma^2}\left(1 + \frac{\tau^2}{4\pi^2}\right), \quad \left[\tau \ll \frac{\pi^2}{(1+2/\gamma)^2}, \gamma \gg 1\right]. \tag{18}$$

Further, we may express the total energy of system in each asymptotic regime as [47],

$$\text{I}: \; \langle \hat{H}\rangle \simeq N\frac{\hbar^2\rho^2}{2m}\left(\gamma - \frac{4}{3\pi}\gamma^{3/2} + \frac{\pi}{12}\frac{\tau^2}{\gamma^{1/2}}\right), \tag{19}$$

$$\text{II}: \; \langle \hat{H}\rangle \simeq N\frac{\hbar^2\rho^2}{2m}\left(\gamma + \frac{\zeta(3/2)}{4\sqrt{\pi}}\tau^{3/2} + \frac{\zeta(1/2)}{2\sqrt{\pi}}\tau^{1/2}\gamma\right), \tag{20}$$

$$\text{III}: \; \langle \hat{H}\rangle \simeq N\frac{\hbar^2\rho^2}{2m}\left(\frac{1}{2}\zeta(3/2) + 2\gamma - \frac{6\gamma^2}{\tau^2}\right), \tag{21}$$

$$\text{IV}: \; \langle \hat{H}\rangle \simeq N\frac{\hbar^2\rho^2}{2m}\left(\frac{\tau}{2} + 2\gamma - \frac{3}{2}\sqrt{\frac{\pi}{2}}\frac{\gamma^2}{\tau^{1/2}}\right), \tag{22}$$

$$\text{V}: \; \langle \hat{H}\rangle \simeq N\frac{\hbar^2\rho^2}{2m}\left(\frac{\tau}{2} + \frac{1}{2}\sqrt{\frac{\pi}{2}}\tau^{1/2} - \sqrt{\frac{\pi}{2}}\frac{\tau^{1/2}}{\gamma}\right), \tag{23}$$

$$\text{VI}: \; \langle \hat{H}\rangle \simeq N\frac{\hbar^2\rho^2}{2m}\left(\frac{\pi^2}{3} - \frac{4\pi^2}{3\gamma} + \frac{\tau^2}{3\gamma}\right), \tag{24}$$

where $\zeta(s)$ is the Riemann zeta function of $s \in \mathbb{R}$.

As described in the main text, the normalized local second-order correlation function may be rearranged and integrated for the total (integrated) correlation function,

$$\overline{G^{(2)}} \equiv \int dz \langle \hat{\Psi}^\dagger(z)\hat{\Psi}^\dagger(z)\hat{\Psi}(z)\hat{\Psi}(z)\rangle = \int_0^L dz g^{(2)}(0)\rho^2. \tag{25}$$

Utilizing the linear density, $\rho = N/L$, this may be expressed as $\overline{G^{(2)}} = N\rho g^{(2)}(0)$, which is used in Eq. (3) of the main text for expressing the exact net work of the uniform 1D Bose gas in terms of $g^{(2)}(0)$.

Exact TBA results.—Experimental realization of a 1D Bose gas often falls outside the asymptotic regimes where analytic approximations are applicable. In such situations, we may utilize the exact Yang-Yang thermodynamic Bethe ansatz [26, 27] to evaluate the equilibrium properties of the gas required for calculating net work and efficiency via Eqs. (1) and (2), respectively. This is presented in Extended Data Fig. 1**a** for experimentally realistic set of system parameters that inhabit the boundary between asymptotic parameter regimes II and III (see Fig. 2). Further, one may utilize the exact TBA to confirm the results derived via approximate analytics in the main text. This is illustrated in Extended Data Figs. 1 **b** and **c**, where we see excellent agreement between these results when the parameters γ and τ are sufficiently deep into the analytic asymptotic regimes.

Maximum efficiency at maximum work.—For a fixed ratio of temperatures, it was noted in the main text that the interaction strength ratio corresponding to maximum work approxi-

mately coincides with that for maximum efficiency, which is uncommon for highly nonequilibrium engine cycles [14, 40]. In the sudden interaction-quench Otto cycle, such coincidence occurs due to the dependence of the total energy of the hot and cold thermal equilibrium states on the interaction strength.

As shown in Eq. (11), the total energy may be separated into its kinetic energy, which scales predominately with temperature, and interaction energy, which scales predominately with interaction strength. Thus, for a fixed ratio of temperatures, τ_h/τ_c, the difference between the total energies of the hot and cold thermal state may be given as a sum of two terms: the first is the kinetic energy difference, determined by the temperature ratio and therefore approximately constant, the second given by the interaction energy difference, which scales with the interaction strengths, γ_h and γ_c, of the hot and cold thermal states as

$$\langle \hat{H}^{int}\rangle_h - \langle \hat{H}^{int}\rangle_c = N\frac{\hbar^2\rho^2}{2m}\left(\gamma_h g_h^{(2)}(0) - \gamma_c g_c^{(2)}(0)\right). \quad (26)$$

However, when operating within a single asymptotic regime under a moderate quench of interaction strength, the $g^{(2)}(0)$ correlation function is only slowly varying with γ. This means, to first approximation, $g_h^{(2)}(0) \simeq g_c^{(2)}(0)$, which in turn transforms the interaction energy difference to

$$\langle \hat{H}^{int}\rangle_h - \langle \hat{H}^{int}\rangle_c \simeq N\frac{\hbar^2\rho^2}{2m}\left(\gamma_h - \gamma_c\right) g_c^{(2)}(0). \quad (27)$$

The heat intake, which is given by Eq. (7), is therefore well approximated by

$$\begin{aligned} Q_1 &= \langle \hat{H}\rangle_h - \langle \hat{H}\rangle_c - \frac{N\hbar^2\rho^2}{2m}(\gamma_h - \gamma_c) g_c^{(2)}(0) \\ &\simeq \langle \hat{H}^{kin}\rangle_h - \langle \hat{H}^{kin}\rangle_c, \end{aligned}$$

which is approximately constant, as detailed above. Therefore, under a fixed ratio of temperatures, the efficiency, which is given by $\eta = W/Q_1$, scales predominately with W, hence $\eta \propto W$.

Isentropic quench.—The conventional isentropic Otto engine cycle is, by definition, fully reversible, and as such obtains the maximum possible values for both net work and efficiency [38]. The isentropic interaction-driven Otto cycle for the uniform 1D Bose gas was introduced in Ref. [18], where they employed the Tomonaga-Luttinger liquid (TLL) theory to derive approximate analytic results for the net work and efficiency. The TLL theory captures the low energy regimes of the uniform 1D Bose gas [48], corresponding to regions I and VI of Fig. 2.

Here, we analyze the performance of the isentropic Otto engine cycle under higher temperatures, i.e., outside of the regime of applicability of the TTL theory. This can be done by utilizing the conservation of entropy condition for the work strokes W_1 and W_2 of Fig. 1 [18], along with the TBA or approximate analytic results for entropy available in the uniform 1D Bose gas [47],

$$\text{I}: \; S \simeq N k_B \left(\frac{\pi}{6}\frac{\tau}{\sqrt{\gamma}} - \frac{\pi^3}{240}\frac{\tau^3}{\gamma^{5/2}}\right), \quad (28)$$

$$\text{II}: \; S \simeq N k_B \left(\frac{3\zeta(3/2)}{4\sqrt{\pi}}\sqrt{\tau} - \sqrt{\gamma} - \frac{\zeta(1/2)}{2\sqrt{\pi}}\frac{\gamma}{\sqrt{\tau}}\right), \quad (29)$$

$$\text{III}: \; S \simeq N k_B \left(\frac{3\zeta(3/2)}{4\sqrt{\pi}}\sqrt{\tau} - \frac{4\gamma^2}{\tau^3}\right), \quad (30)$$

$$\text{IV}: \; S \simeq N k_B \left(\ln\left(\frac{\sqrt{\tau}}{2\sqrt{\pi}}\right) + \frac{3}{2} + \frac{\sqrt{\pi}}{\sqrt{2\tau}} - \frac{1}{2}\sqrt{\frac{\pi}{2\tau^3}}\gamma^2\right), \quad (31)$$

$$\text{V}: \; S \simeq N k_B \left(\ln\left(\frac{\sqrt{\tau}}{2\sqrt{\pi}}\right) + \frac{3}{2} + \frac{\sqrt{\pi}}{\sqrt{2\tau}} + \frac{2}{\gamma} + \frac{\sqrt{\pi}}{\gamma\sqrt{2\tau}}\right), \quad (32)$$

$$\text{VI}: \; S \simeq N k_B \left(\frac{\tau}{6} + \frac{\tau^3}{45\pi^2} + \frac{2\tau}{3\gamma} + \frac{2\tau}{3\gamma^2}\right). \quad (33)$$

In Extended Data Fig. 2 we demonstrate performance of the isentropic engine cycle (using the analytic results), which may be directly compared against that of the sudden quench engine cycles explored in Fig. 3 of the main text. Notably, over the range of parameters that the sudden quench Otto cycle operates as an engine, its performance remains relatively close in both net work and efficiency to the comparative isentropic results, despite being highly nonequilibrium and thus irreversible. However, further optimization of the sudden quench Otto cycle is beyond the scope of this work.

Thermal operation regimes.—Under large interaction strength quenches, for fixed temperatures τ_c and τ_h, it was noted in the main text that the heater is the inevitable mode of operation. This scenario requires the fulfilment of two conditions: the work in, W_1, exceeds the energy gap between the hot and cold thermal states, whereas the work out, W_2, remains less than this same gap (see Fig. 4 **d**). As detailed above, in the section on maximum efficiency at maximum work, the total energy difference between the hot and cold thermal states for fixed temperature ratios, τ_h/τ_c, is given by a sum of the kinetic energy difference, which is approximately constant, and the interaction energy difference, given by Eq. (26).

Here, for a *large* quench in interaction strength, the correlation function is no longer approximately constant, and $g_h^{(2)}(0)$ is strongly monotonically decreasing as a function of γ_h, i.e. $g_h^{(2)}(0) < g_c^{(2)}(0)$. We therefore find that the work input, W_2, exceeds the interaction energy difference given in Eq. (26),

$$W_2 \propto (\gamma_h - \gamma_c) g_c^{(2)}(0) > \gamma_h g_h^{(2)}(0) - \gamma_c g_c^{(2)}(0). \quad (34)$$

Further, as the kinetic energy term is approximately constant, W_2 inevitably exceeds the difference in total energy between the hot and cold thermal states due to its linear dependence on γ_h.

Similarly, since $g_h^{(2)}(0)$ monotonically decreases with γ_h for large quenches of interaction strength, the magnitude of

the work output, $|W_1| \propto (\gamma_h - \gamma_c) g_h^{(2)}(0)$, remains less than the energy gap between the hot and cold thermal states:

$$|W_1| \propto (\gamma_h - \gamma_c) g_h^{(2)}(0) < \gamma_h g_h^{(2)}(0) - \gamma_c g_c^{(2)}(0). \quad (35)$$

These two conditions, taken together, imply operation as a heater under large interaction quenches.

In contrast, for any fixed value of γ_c and γ_h, an increasingly higher temperature of the hot thermal state, τ_h, means that the corresponding correlation function, $g_h^{(2)}(0)$, monotonically increases towards its maximum value of $g_h^{(2)}(0) \simeq 2$, which is achieved in regime IV, defined in Eq. (16). Thus, there is always a value of τ_h such that $g_h^{(2)}(0) > g_c^{(2)}(0)$, turning the Otto cycle into the engine operation regime.

Finally, in the refrigerator thermal operation regime, for $\tau_h = \tau_c$ and an infinitesimal quench of interaction strength, $\gamma_h - \gamma_c = \delta\gamma$, the net work vanishes as $W \propto (\gamma_h - \gamma_c)(g_h^{(2)}(0) - g_c^{(2)}(0)) \propto \delta\gamma^2$. This occurs as the zeroth order terms in the correlation function cancel when taking their difference in a single asymptotic regime. In contrast, the heat intake, Q_1, depends on the difference in total energy, which to first order vanishes as $Q_1 \propto \delta\gamma$. This results in $\mathrm{CoP[R]} = |Q_1|/W - 1 \propto \delta\gamma^{-1}$, which diverges as $\delta\gamma \to 0$, as noted in the main text.

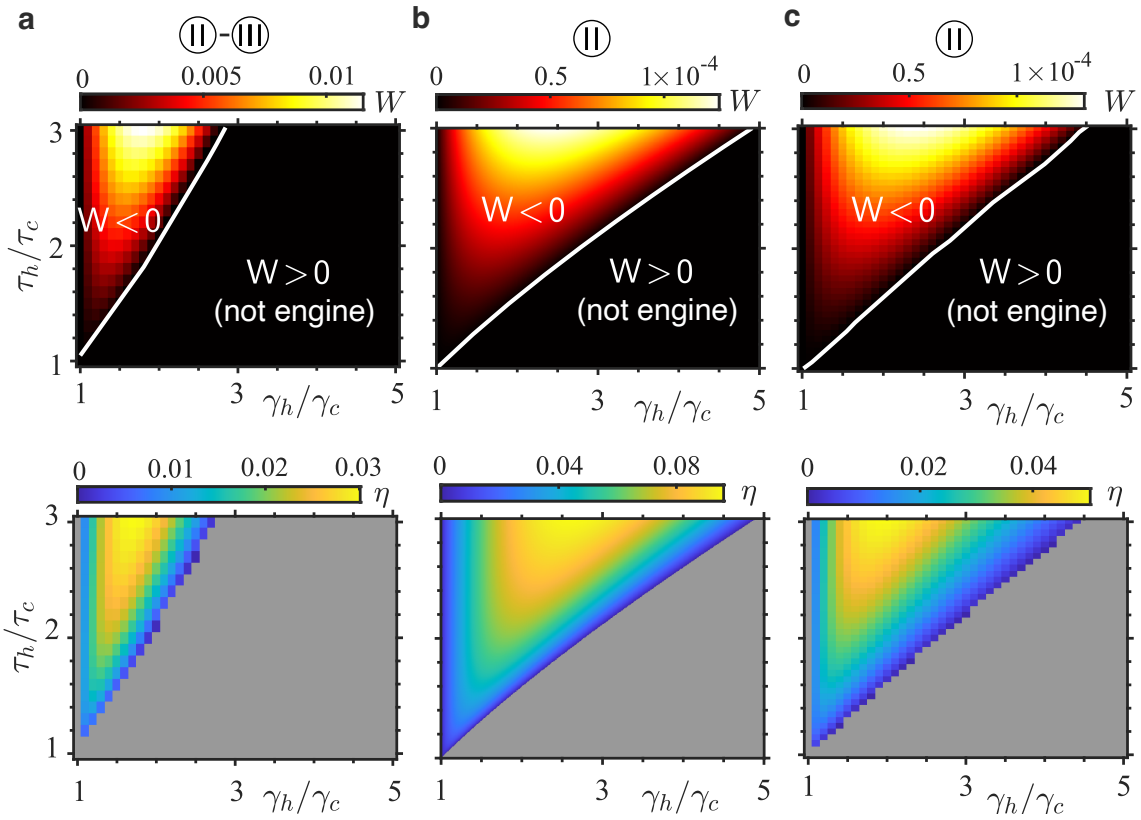

Extended Data FIG. 1. Performance of the sudden interaction quench quantum Otto cycle, numerically evaluated via the thermodynamic Bethe ansatz. Panel **a** demonstrates numerically evaluated net work and efficiency for a system with a cold thermal state defined by $\gamma_c = 0.1$, $\tau_c = 0.5$, lying on the border of regimes II and III (see Fig. 2), and thus lying outside the range of the analytic approximations utilized in the main text. Panel **b** is a copy of Fig. 3**a** for comparison with the numerical evaluation of the same cycle in panel **c** using the TBA. Here, there is excellent agreement in the net work between panels **b** and **c**, with small disagreement under large interaction strength and temperature ratios, as the hot thermal state is approaching the edge of the asymptotic regime where it is applicable.

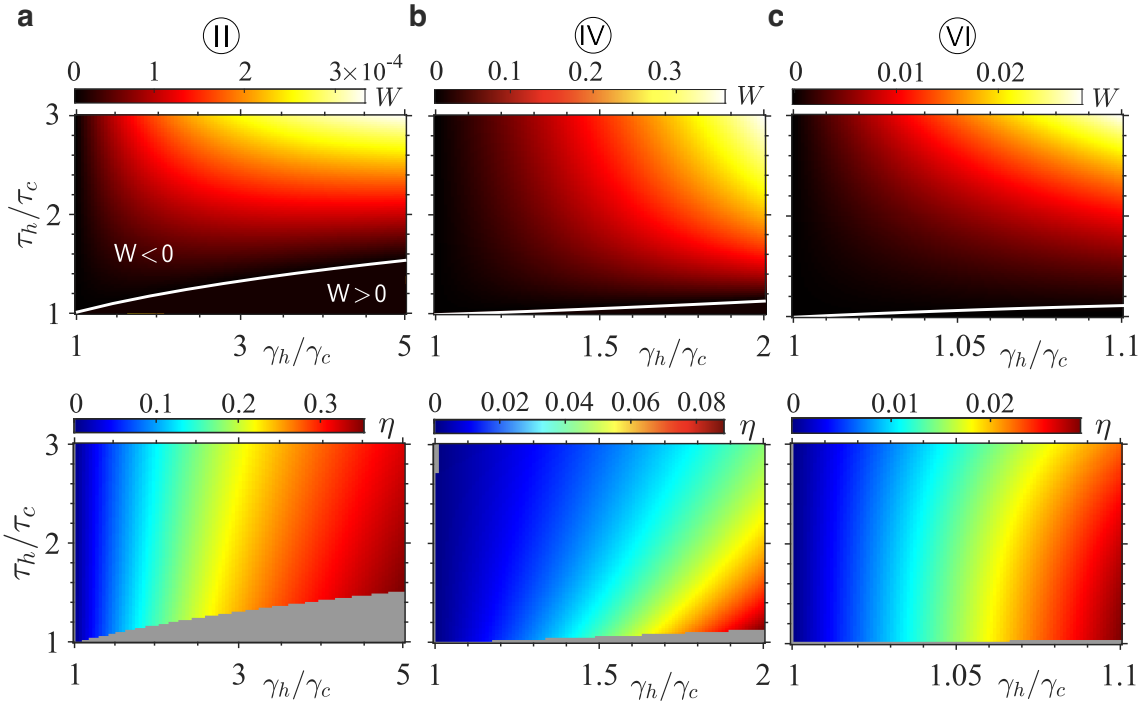

Extended Data FIG. 2. Performance of the isentropic interaction-driven quantum Otto cycle, for the same parameters as in the sudden quench scenarios of Figs. 3 **a**–**c**. As one approaches the boundary of the engine regime, defined by $W = 0$, the efficiency, which is given by the ratio of the net work, W, to the heat intake, Q_1, is approximately constant, unlike the W itself which approaches 0 near the boundary. However, as the efficiency is only a valid metric in the engine regime, it is set to gray scale outside the engine regime.